Chemical Physics 428 (2014) 164–174

Contents lists available at ScienceDirect

Chemical Physics

journal homepage: www.elsevier.com/locate/chemphys

On the stability and dynamics of (sulfuric acid)(ammonia) and (sulfuric acid)(dimethylamine) clusters: A first-principles molecular dynamics investigation

V. Loukonen [a,*], I-F.W. Kuo [b], M.J. McGrath [c,1], H. Vehkamäki [a]

[a] Department of Physics, University of Helsinki, P.O. Box 64, FI-00014 University of Helsinki, Finland
[b] Lawrence Livermore National Laboratory, Chemical Sciences Division, Livermore, CA 94550, USA
[c] Department of Biophysics, Graduate School of Science, Kyoto University, Kyoto 606-8502, Japan

ARTICLE INFO

Article history:
Received 11 September 2013
In final form 19 November 2013
Available online 1 December 2013

Keywords:
Weakly bound molecular clusters
First-principles molecular dynamics
Electric dipole moment
Sulfuric acid
Atmospheric new-particle formation

ABSTRACT

The main pathway of new-particle formation in the atmosphere is likely to begin from small sulfuric acid clusters stabilized by other compounds, such as ammonia or amines. Here, we present the results of first-principles molecular dynamics simulations probing the stability and dynamics of (sulfuric acid)(ammonia/dimethylamine) clusters with two, three and four sulfuric acid molecules and a varying number of the bases. In each of the eight simulated clusters, an energetic equilibrium was reached and 35 ps of equilibrium data was collected in the $NVT(T = 300\ \mathrm{K})$ ensemble. The clusters exhibited pronounced thermal motion including rotations of the molecules within the clusters. Regardless of the continuous movement, the clusters stayed bound together. The calculated electric dipole moments were found to be sensitive to the thermal motion and consequently, large fluctuations were observed. In addition, the vibrational spectra for all the clusters were determined, indicating that the thermal motion differs from purely harmonic motion.

1. Motivation

Currently, one of the most pressing research problems the scientific community faces is the formation and growth of atmospheric aerosol particles. For example, some of these tiny particles take part in the processes deteriorating the quality of air, directly affecting the daily lives of millions of people [1]. On a grander scale, aerosol particles are intimately tied to the climate and climate change via different radiative processes [2]. The numerous and interconnected feedback mechanisms, ranging over several orders of magnitude in space and time, make aerosol particle formation and its consequences very elusive to study, both experimentally and theoretically [3]. Here, we adapt bottom-up approach to tackle the phenomenon: we present results from first-principles molecular dynamics simulations of atmospheric sulfuric acid clusters – thus concentrating on the smallest space and time regimes of sub-nanometer and -nanosecond.

The main driving agent of new-particle formation in the atmosphere is sulfuric acid [4,5]. However, the measured ambient concentrations of sulfuric acid are several orders of magnitude too small for it to alone explain the observed new-particle formation events and the acid alone does not account for most of the further aerosol particle growth either [6,7]. Traditionally, the explanation for the observations has been sought from some combination of sulfuric acid, water and ammonia "nucleating particles" [8]. The role of ions has also been extensively discussed [9,10]. However, state-of-the-art laboratory measurements concluded that sulfuric acid particle formation enhanced by ammonia and ions cannot explain the boundary-layer formation events [11]. Recently, the participation of various amines in the process has drawn a lot of attention. Theoretical studies, motivated by filter sample findings [12], first suggested that amines, such as dimethylamine, stabilize the smallest sulfuric acid clusters much more strongly than the standard candidate ammonia, and thus possibly enhance the particle formation more effectively [13,14]. The suggestion was later strengthened by various experiments, and further experimental and theoretical work has studied the clusters of sulfuric acid and amines [15–22]. The current paper continues this line of research: we focus on the dynamics and stability of sulfuric acid–ammonia and sulfuric acid–dimethylamine clusters.

The bulk of the previous theoretical studies have been static structure optimization calculations [23]. In such calculations, one typically tries to find the global minimum energy cluster as a function of the molecular coordinates, that is, to find the arrangement of the molecules in the cluster which minimizes the electronic

* Corresponding author. Tel.: +358 503182219.
E-mail address: ville.loukonen@helsinki.fi (V. Loukonen).
[1] Present address: Laboratoire des Sciences de la Climat et l'Environment, 91191 Gif-sur-Yvette, France.

0301-0104/$ - see front matter © 2013 Elsevier B.V. All rights reserved.
http://dx.doi.org/10.1016/j.chemphys.2013.11.014

ground state energy. Once such a cluster is found, all the molecular vibrations are often assumed to be harmonic. In addition, the clusters are most often assumed to rotate rigidly and the translational degrees of freedom are taken to be those of an isolated ideal gas particle. The partition function is then constructed under these assumptions, yielding various thermodynamical quantities via the machinery of statistical mechanics. This scheme includes the temperature and entropy into the electronic structure calculations, thus effectively interpolating the results from $T = 0$ K to, say, $T = 300$ K. The main shortcoming of the scheme is the lack of detailed and non-ideal descriptions of the kinetic energy contributions. To address this issue and to obtain insight on how the small clusters behave when the temperature and the kinetic energy are explicitly taken into account, we performed first-principles molecular dynamics (FPMD) simulations. One prior attempt has been performed to use FPMD on atmospheric (sulfuric acid)(base) clusters [24]. In that investigation, the threshold of proton transfer in hydrated sulfuric acid clusters (up to two acid molecules with six water molecules) with various bases was studied. The results differed partly from standard quantum chemical results [14], possibly due to the dynamical effects, demonstrating that dynamics of atmospheric sulfuric acid clusters should be studied in more detail.

Here, we extend the body of atmospherically relevant FPMD simulations in both size and simulation time: the largest cluster studied here contains four sulfuric acid and four dimethylamine molecules, and equilibrium data was collected for all the clusters for 35 ps (the simulation details are given in Section 2). To achieve this, one compromise had to be made: the exclusion of water. Although in the atmosphere there are several orders of magnitude more water than sulfuric acid, ammonia or dimethylamine, not much is currently known about the hydration state of the clusters formed by the latter molecules. Agreeably, FPMD would be a good method to investigate the role of water in the clusters, especially as water is often lost from small clusters during detection in the experiments. However, the inclusion of water molecules would increase the computational cost and complexity significantly, and thus it is left for future studies. Furthermore, as the main goal of the present paper is to study the dynamics and stability of sulfuric acid clusters, the exclusion of water might be a good first order approximation as the binding of sulfuric acid with water is considerably weaker than with ammonia or dimethylamine.

2. Simulations

We performed Born–Oppenheimer based first-principles molecular dynamics simulations, where the atomic nuclei evolve in time according to the classical equations of motion. However, the forces driving the dynamics are calculated from electronic structure theory [25,26]. All the simulations were performed using the CP2K program package (www.cp2k.org) and the forces were calculated within Kohn–Sham density functional theory as implemented in the Quickstep [25] module of CP2K. We used the PBE functional [27], which has been previously shown to work well for polar hydrogen-bonding liquids [28,29] and recently in the context of atmospheric clusters [30,31]. The density functional was used with a dual basis set method [26]: a doubly polarized triple-ζ Gaussian-type basis set in real-space and a plane-wave basis set with a cut-off of 600 Ry in the momentum-space. Norm-conserving GTH pseudo-potentials were used for the core electrons [32]. The convergence criteria for the wavefunction was 10^{-7} Hartrees. The size of the simulation box was $20 \times 20 \times 20$ Å^3 in all of the simulations.

Once the forces were obtained, the system was propagated in time with a timestep of 0.5 fs in the canonical *NVT* ensemble. The temperature was set to the ambient $T = 300$ K where every degree of freedom was controlled by individual Nosé–Hoover chain thermostats [33] with a coupling constant of 2000 cm^{-1}. The canonical ensemble was chosen as we wanted to observe how the small clusters behave under constant temperature. Especially, we were interested to see how the presumably stable clusters responded when the system possessed kinetic energy at $T \neq 0$ K conditions. Guided by a recent quantum chemical study [18], which extensively searched for the most stable molecular clusters, we chose six (sulfuric acid)$_m$(base)$_n$ clusters (with $m = 2, 3, 4$) separately with the two base molecules, ammonia and dimethylamine (henceforth, sulfuric acid will be abbreviated as SA, ammonia as Amm and dimethylamine as DMA). In this size range, the (SA)$_m$(Amm)$_n$ clusters with $n = m - 1$, and the clusters of (SA)$_m$(DMA)$_n$ with $n = m$ were found to be the most stable ones [18]. In addition to these six clusters, we included the clusters of (SA)$_3$(Amm)$_3$ and (SA)$_2$(DMA)$_1$ into this study, as the stability of these clusters was very close to the most stable ones [18], and further, it extended our data set in a way that we were able to directly compare the roles of the base molecules in the clusters of (SA)$_2$(base)$_1$ and (SA)$_3$(base)$_3$.

We took the initial geometries from the literature [18] and optimized the clusters with the level of theory used in the simulations. While it is true in general that the minima found with different methods are not necessarily the same, here this matter is of secondary importance: the optimized initial clusters were only used as starting points for the equilibration simulations. To be able to draw meaningful physical conclusions based on the simulations, the clusters need to be first equilibrated. Thus, only after the clusters had successfully reached an energetic equilibrium, 35 ps production run simulations were performed. All the analysis is based on the production runs. The results of the simulations are presented in the following section: first, we discuss the energetic and structural properties observed in the simulations, after which we focus on the electric dipole moments and on the vibrational–rotational spectra.

3. Results and discussion

3.1. Energetics and structural considerations

One of the motivating questions behind this investigation was to find out how the presumably stable atmospheric small clusters behave if the temperature is taken into account explicitly. One fundamental way to answer this question is to look at the energetics of the clusters. In Figs. 1 and 2 one can see the potential energy as a function of time over the whole trajectory for all the studied ammonia- and amine-containing clusters, respectively. There are at least two interesting features to notice.

First, an energetic equilibrium is reached in all of the clusters. Typically, this happened within a few picoseconds. The only cluster not to equilibrate within ten picoseconds, was the cluster of (SA)$_4$(Amm)$_3$. Curiously, even 45 ps was not enough to relax the structure. Intrigued by this, the simulation was continued. The cluster finally reached an equilibrium after ~55 ps. To ascertain this, and to collect equilibrium data for the cluster, the simulation was continued for another 35 ps.

In general, the bonding patterns in the studied clusters are largely dictated by proton transfers from sulfuric acid molecules to the base molecules. The proton transfers create ion pairs within the electrically neutral clusters and the resulting hydrogen bonds are relatively strong. In all of the initial starting structures, the base molecules had accepted one proton from the acids. In other words, all the ammonia molecules NH_3 were in the form of NH_4^+ and all the dimethylamine molecules $(CH_3)_2NH$ were in the form of $(CH_3)_2NH_2^+$, that is, as ammonium and dimethylaminium ions,

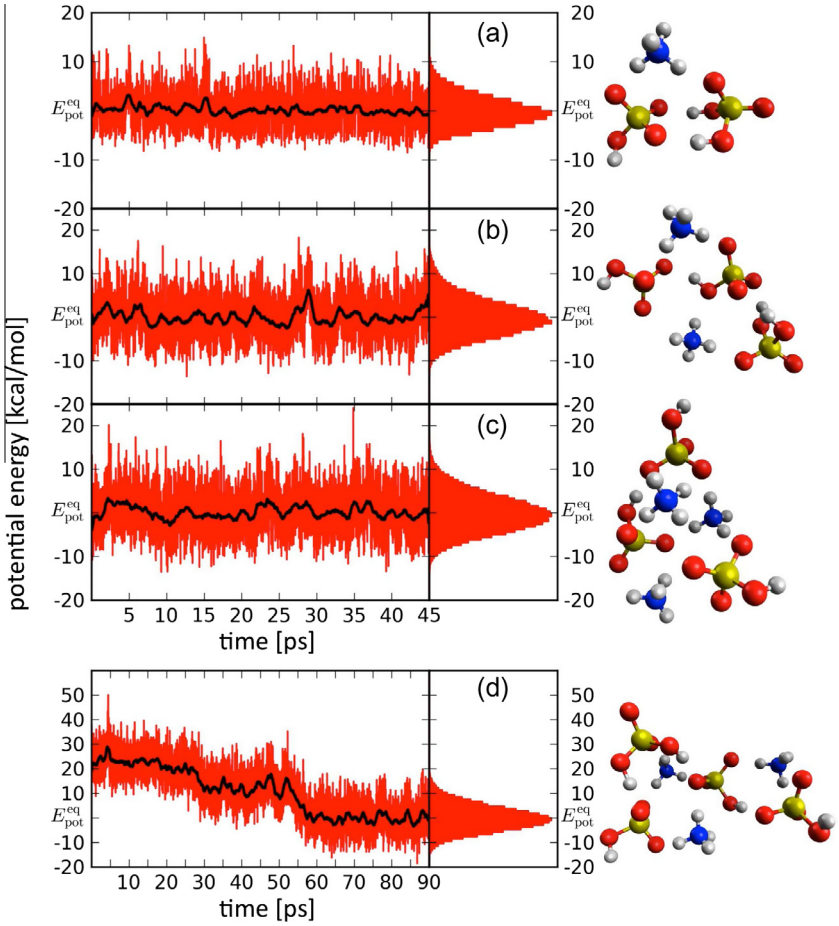

Fig. 1. Potential energy as a function of time for the ammonia-containing clusters at the temperature $T = 300$ K: (a) $(SA)_2(Amm)_1$, (b) $(SA)_3(Amm)_2$, (c) $(SA)_3(Amm)_3$, (d) $(SA)_4(Amm)_3$. The histograms show the potential energy distributions during the equilibrium simulations (from 10 ps to 45 ps), where E_{pot}^{eq} is the mean value of the potential energy at equilibrium. The black curve shows a sliding average of the potential energy with a 1 ps resolution. Note that for the cluster of $(SA)_4(Amm)_3$ the time axis is longer; for this cluster the equilibrium period is from 55 ps to 90 ps. The balls-and-sticks figures show the structures of the clusters at the time 27.5 ps (for the $(SA)_4(Amm)_3$ cluster at 72.5 ps); sulfur atoms are pictured in yellow, oxygen in red, nitrogen in blue, carbon in grey and hydrogen in white. (For interpretation of the references to colour in this figure caption, the reader is referred to the web version of this article.)

respectively. Correspondingly, there were an equal amount of sulfuric acid molecules H_2SO_4 as bisulfate ions HSO_4^- in the clusters. The importance of the proton transfers for the stability of the these clusters has been seen in a number of previous first-principles studies [13,14,18,19,24]. Indeed, the high reactivity of sulfuric acid is probably one of the main reasons why it has such an important role in atmospheric new-particle formation.

Besides $(SA)_4(Amm)_3$, the other two clusters which did not equilibrate immediately were $(SA)_3(DMA)_3$ and $(SA)_4(DMA)_4$. The structural changes in any of these clusters during the equilibration period were not large; in fact, the structural reorganization was rather subtle. However, these minute changes in geometries do have a significant effect in the potential energy (cf. Figs. 1 and 2). This highlights the advantageous features of molecular dynamics. Even for these relatively small molecular clusters, it is already a very challenging task to find the minimum energy geometries at $T = 0$ K. Guessing the cluster structures for $T = 300$ K is yet more difficult, if not impossible, without real dynamical simulations. It should be stressed that during the equilibration there were no proton transfers – the changes in the potential energy arise from molecules finding more optimal bonding patterns.

Secondly, the potential energy is constantly oscillating in all of the clusters. Furthermore, the maximum magnitude of the oscillation is ~10 kcal/mol and is not dependent on the cluster composition or whether the equilibrium is reached or not. Indeed, this is what one would expect: the kinetic energy at the temperature of $T = 300$ K keeps the molecules constantly moving. This thermal motion shows as oscillation in the potential energy, and produces distributions centered around the equilibrium values (cf. distributions in Figs. 1 and 2 and the numerical values in Table 1). The temperature distributions over the entire trajectories are shown in Fig. 3. The obtained distributions are centered at the target temperature of $T = 300$ K confirming that the thermostatting is working properly. It is also noteworthy that none of the temperature distributions show multiple peaks – this is in accordance with the notion that the magnitude of the potential energy oscillation is the same throughout the simulation runs.

The potential energy distributions during the equilibrium simulations provoke interesting considerations. From a cluster point-of-view the physical interpretation is clear: at the temperature of $T = 300$ K there exists a distribution of molecular geometries for each of the studied clusters – likely to be true in general also. One might argue, that in some sense the concept of "global minimum energy structure" is not too meaningful at ambient temperatures; obtaining thermodynamical quantities via the usual machinery of statistical physics from the global minimum energy structures within the harmonic approximation may lead to substantial errors as the kinetic energy contribution is not explicitly considered. In Table 1 the potential energies E_{pot}^{eq} from the simulations are shown relative to the potential energies calculated at the

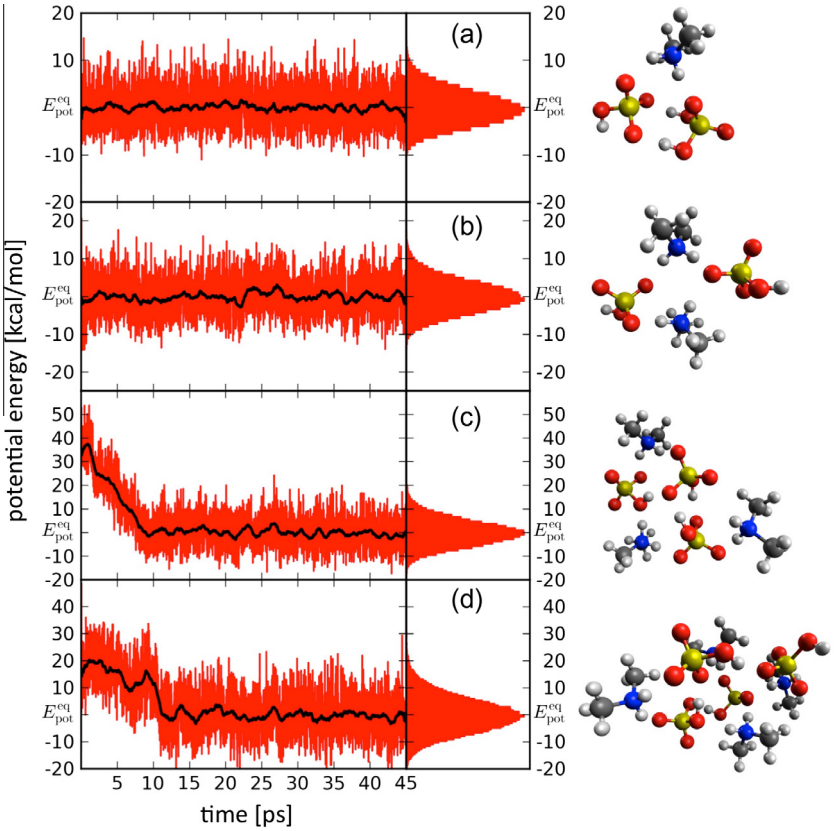

Fig. 2. Potential energy as a function of time for the amine-containing clusters at the temperature $T = 300$ K: (a) $(SA)_2(DMA)_1$, (b) $(SA)_2(DMA)_2$, (c) $(SA)_3(DMA)_3$ and (d) $(SA)_4(DMA)_4$. The histograms show the potential energy distributions during the equilibrium simulations (from 10 ps to 45 ps), where E^{eq}_{pot} is the mean value of the potential energy at equilibrium. The black curve shows a sliding average of the potential energy with a 1 ps resolution. The balls-and-sticks figures show the structures of the clusters at the time 27.5 ps; sulfur atoms are pictured in yellow, oxygen in red, nitrogen in blue, carbon in grey and hydrogen in white. (For interpretation of the references to colour in this figure caption, the reader is referred to the web version of this article.)

Table 1
Mean values of the potential E^{eq}_{pot} and kinetic energy E^{eq}_{kin} after equilibration (last 35 ps of the simulations). The potential energy values are relative to the potential energies of the corresponding optimized structures at $T = 0$ K.

Cluster	E^{eq}_{pot} [kcal/mol]	E^{eq}_{kin} [kcal/mol]
$(SA)_2(Amm)_1$	14.4 ± 3.0	16.0 ± 3.1
$(SA)_3(Amm)_2$	20.9 ± 4.2	25.9 ± 3.9
$(SA)_3(Amm)_3$	25.7 ± 4.3	29.5 ± 4.2
$(SA)_4(Amm)_3$	7.4 ± 5.1	35.8 ± 4.5
$(SA)_2(DMA)_1$	20.6 ± 3.5	21.4 ± 3.6
$(SA)_2(DMA)_2$	27.8 ± 4.2	30.4 ± 4.3
$(SA)_3(DMA)_3$	15.0 ± 5.4	45.6 ± 5.2
$(SA)_4(DMA)_4$	19.0 ± 6.5	60.8 ± 6.0

same level of theory at $T = 0$ K. Table 1 also contains the kinetic energies E^{eq}_{kin} obtained from the simulations. Comparing the values of these two quantities reveals that $E^{eq}_{pot} \neq E^{eq}_{kin}$, indicating that there is anharmonicity in the energetics of the clusters in dynamical equilibrium at $T = 300$ K.

However, an accurate assessment of the dynamical effects and the anharmonicity on the various thermodynamical quantities, such as the formation free energies, is extremely difficult. In this particular study there were no drastic differences in the cluster structures during the simulation compared to the stable static geometries. This might be partly due to the nature of the clusters. As already mentioned, the proton transfers and the subsequent hydrogen bonding patterns between the ion pairs seem to quite decisively dictate the geometries of the clusters. Colloquially, the clusters are looser during the simulations – in particular, the intermolecular bond lengths and angles are continuously evolving. The magnitude of the fluctuation in the distances was moderate and rather uniform throughout the simulations. Fig. 4 shows the radii of gyrations (the average distance from the center of mass), the center-of-mass radii (the largest distance from the center of mass) and the physical radii (half of the largest separation between the atoms) for all the clusters. One can see that the physical dimensions are rather stable.

The physical size of the clusters bears some significance in the growth kinetics. Modeling approaches where the collisions between the molecules and/or clusters are not explicitly considered depend on the bulk values of the molecular and cluster sizes. For example, in kinetic modeling ([34, e.g.]) the colliding molecules and clusters are often assumed to be spherical "liquid droplets" and typically the hard-spheres collision cross sections are used to approximate the collision rates. The hard-spheres collision cross section is proportional to the square of the sum of the radii of the colliding molecules or clusters and thus it is desirable to use as realistic radii as possible. The simulations presented here enable a comparison between the first-principles molecular dynamics radii and the bulk radii. The "liquid drop model" radii together with (hypothetical) electrical mobility radii are shown in Fig. 4. The electrical mobility radius approximates the size at which several instruments would detect the clusters [35]. Comparing the liquid drop model radii to the physical and center-of-mass radii obtained from the simulations reveals that the liquid drop radii differ from these by an average 0.6 Å and 0.9 Å, respectively. In terms of hard-spheres collision cross sections, in the worst case the differences in radii turn into a discrepancy factor of 1.8 in the collisions

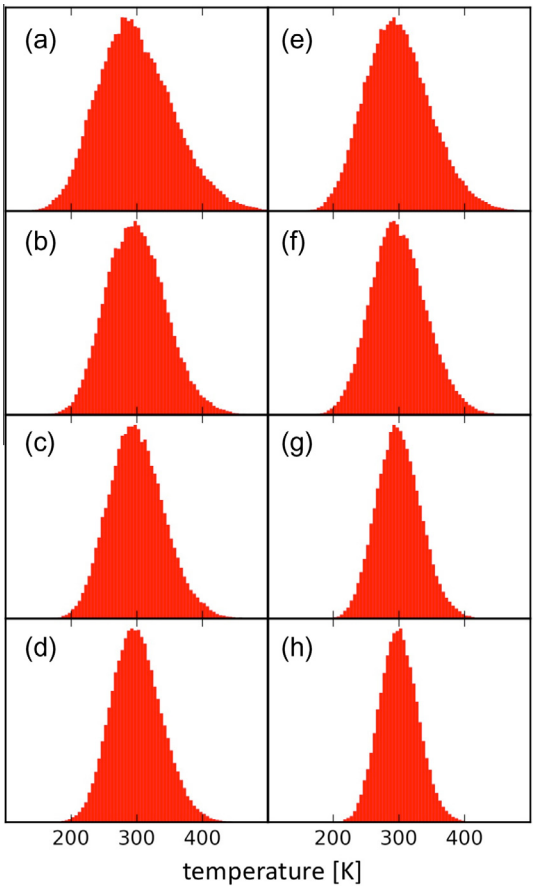

Fig. 3. Temperature distributions of all the studied clusters for the whole length of the simulations. (a) $(SA)_2(Amm)_1$, (b) $(SA)_3(Amm)_2$, (c) $(SA)_3(Amm)_3$, (d) $(SA)_4(Amm)_3$, (e) $(SA)_2(DMA)_1$, (f) $(SA)_2(DMA)_2$, (g) $(SA)_3(DMA)_3$ and (h) $(SA)_4(DMA)_4$.

between the clusters examined here. The bulk approach with an error smaller than a factor of two is a fairly good approximation for the collision cross sections. However, it should be kept in mind that for real molecules and clusters the electronic interactions have larger range than the sharp boundary of a liquid droplet, and it is likely that more crucial uncertainties arise from other aspects of the collision process, such as the sticking factor or cluster rearrangement and fragmentation after collisions.

In addition to showing the fluctuation in the size of the clusters, more information can be extracted from Fig. 4. Comparing the radii of gyrations to the physical radii, one can see how the mass is distributed in the clusters. For example, the physical radii of the two smallest clusters, $(SA)_2(Amm)_1$ and $(SA)_2(DMA)_1$, are roughly equal. However, the radii of gyrations reveal that the mass in $(SA)_2(DMA)_1$ is more dispersed, yielding thus a larger radius of gyration. Conversely, the radii of gyration of the $(SA)_3(DMA)_3$ and $(SA)_4(DMA)_4$ clusters are very similar, but the physical radius of the $(SA)_4(DMA)_4$ is clearly larger. However, the mass must be distributed in a similar fashion in these clusters (cf. the molecular structures in Fig. 2).

A more detailed cluster point-of-view can be obtained by studying radial distribution functions (RDFs). For the molecular clusters in this study, the most interesting RDFs are those between the sulfur atoms and the ones between the sulfur and the nitrogen atoms. The former yields information on how the sulfuric acid molecules coordinate each other and the latter how the acids and bases are coordinated in the clusters. These RDFs for all the studied clusters can be seen in Fig. 5. Fig. 5 shows how the oscillation in energy translates into oscillation in distances; spikes of the stable static structures (shown in Fig. 5 in black) turn into distributions, showing that the distances can, on the average, either increase or decrease when the clusters undergo thermal motion. In addition, the asymmetry in the clusters of $(SA)_3(Amm)_2$ and $(SA)_4(Amm)_3$ – caused by one intact sulfuric acid molecule – can be clearly seen in the sulfur–sulfur RDFs. Interestingly, adding one ammonia molecule to the former cluster leads to a tighter geometry, as can be seen in the $(SA)_3(Amm)_3$ sulfur–sulfur RDF. However, even with the same numbers of acid and base molecules this cluster is not geometrically symmetric, unlike its amine-containing counterpart, cf. (c) and (g) in Fig. 5. In the $(SA)_3(DMA)_3$ cluster each of the amines is coordinated by two acids. In the corresponding ammonia cluster, two of the ammonia molecules are coordinated by three acid molecules and the one remaining base is coordinated by two

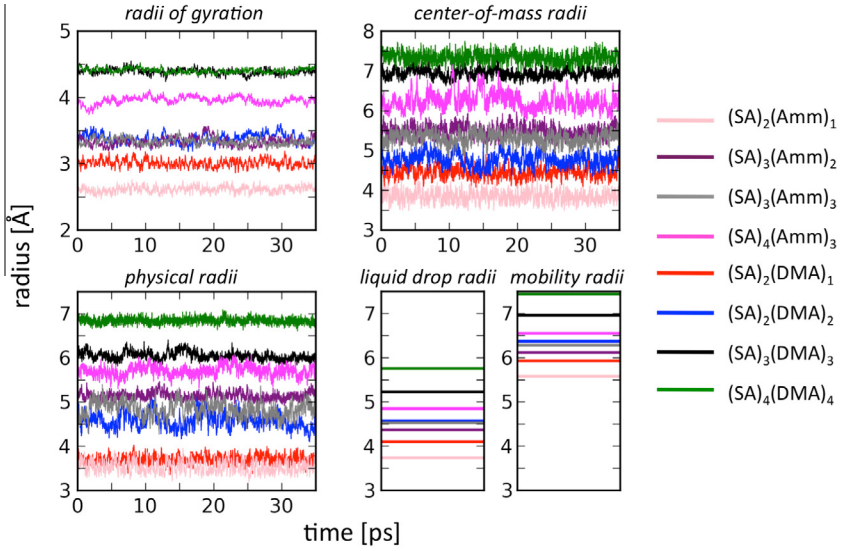

Fig. 4. The radii of gyration, the center-of-mass radii and the physical radii for all the studied clusters (see definitions in the text). The radii are given in Ångströms and the time corresponds to the last 35 ps of the simulation runs. For comparison, the liquid drop model radii r_{ldm} and the hypothetical electrical mobility radii [35], $r_{mobi} = (r_{ldm} + 1.5\text{Å})\left(1 + \frac{28.8\ u}{m_{cluster}}\right)^{1/2}$ where u is the atomic mass unit, are shown as well. The bulk densities needed for r_{ldm} and r_{mobi} are taken from the CRC Handbook of Chemistry and Physics [36].

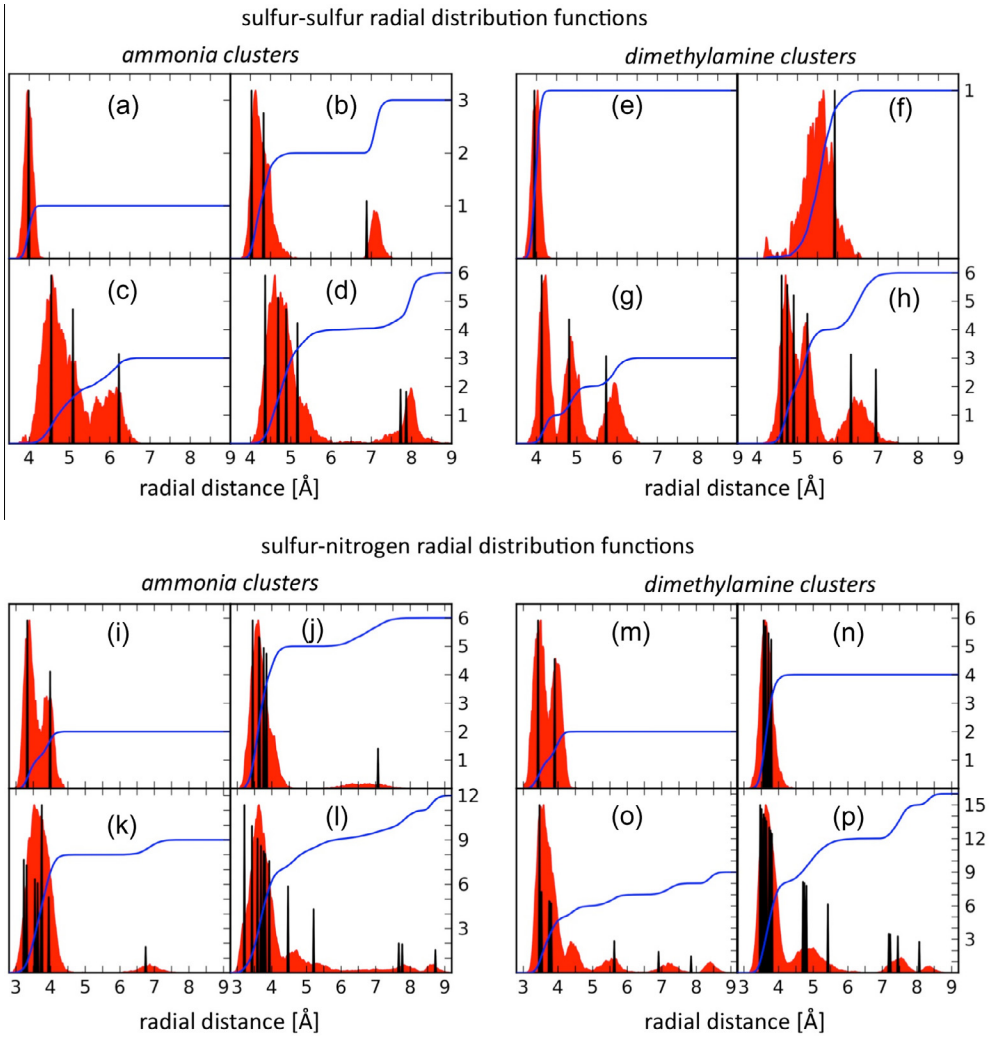

Fig. 5. The sulfur–sulfur and sulfur–nitrogen radial distribution functions (RDFs) of all the studied clusters are shown in red (in arb. units). For comparison, the RDFs of the optimized, static clusters are plotted in black. The blue curves show the coordination numbers (CNs). The CNs measure how many pairs of S–S and S–N atoms are within the radial distance (indicated on the right-hand side ordinate). The static geometries were obtained by optimizing the cluster structures, taken from the equilibrium simulations, at the same level of theory as used in the simulations. (a)&(i) $(SA)_2(Amm)_1$, (b)&(j) $(SA)_3(Amm)_2$, (c)&(k) $(SA)_3(Amm)_3$, (d)&(l) $(SA)_4(Amm)_3$, (e)&(m) $(SA)_2(DMA)_1$, (f)&(n) $(SA)_2(DMA)_2$, (g)&(o) $(SA)_3(DMA)_3$ and (h)&(p) $(SA)_4(DMA)_4$. (For interpretation of the references to colour in this figure caption, the reader is referred to the web version of this article.)

acids. Even though both of the base molecules are able to accept one proton, the number of hydrogen bonds they can participate in is different. Within the clusters ammonia can form up to four bonds, whereas dimethylamine only two. This fact is already significant in the small clusters studied here, but the importance is likely to grow with the size of the clusters. From the structures of the clusters in Fig. 2, one can see that the amine-containing clusters are quite "closed" – what sticks out are the inert methyl groups, especially in $(SA)_3(DMA)_3$ and $(SA)_4(DMA)_4$ clusters. On the other hand, in the ammonia clusters there are "free" hydrogens, potentially available for bonding (cf. Fig. 1).

The simulations also revealed some unexpected dynamical structural behavior. After the clusters had reached equilibrium bonding patterns, these patterns did not change. However, the individual atoms participating in the hydrogen bonds did change. In other words, the molecules in the clusters did not only exhibit thermal vibrations, but also rotations. These concerted rotations were confined by the equilibrium bonding patterns and the symmetry of the molecules. In the ammonia-containing clusters, the rotating species were mainly the singly-protonated ammonium ions, which are very symmetric. In the dimethylamine clusters the rotating molecules were the singly-deprotonated bisulfate ions, where the three free oxygen atoms are symmetric with respect to the center sulfur atom. These rotations can be seen as abrupt changes of the participating atoms in the N–H···O bond distances in Figs. 6 and 7, where the former shows this bond fluctuation in the cluster of $(SA)_3(Amm)_2$ and the latter in the cluster of $(SA)_2(DMA)_2$.

Regardless of the oscillation, vibration and rotation, during the simulations there were no signs of clusters breaking up. Nor were there any signs of donated protons transferring back to bisulfate ions from either of the base molecules. This is one of the most important results of the current paper as the stability of the clusters depends on the proton transfers. Consequently, it is very unlikely that any molecule involved in the proton-transfer-induced ion pair would leave the cluster, and accordingly, this was not observed. In particular for the clusters with an equal number of acids and bases, this suggests that the smallest unit to evaporate would be $(SA)_1(base)_1$. However, also this type of cluster break-up seems to be hindered by the geometry of the studied clusters: both the acid and base molecules are coordinated by more than just one molecule of the other kind. This holds for the other clusters as well:

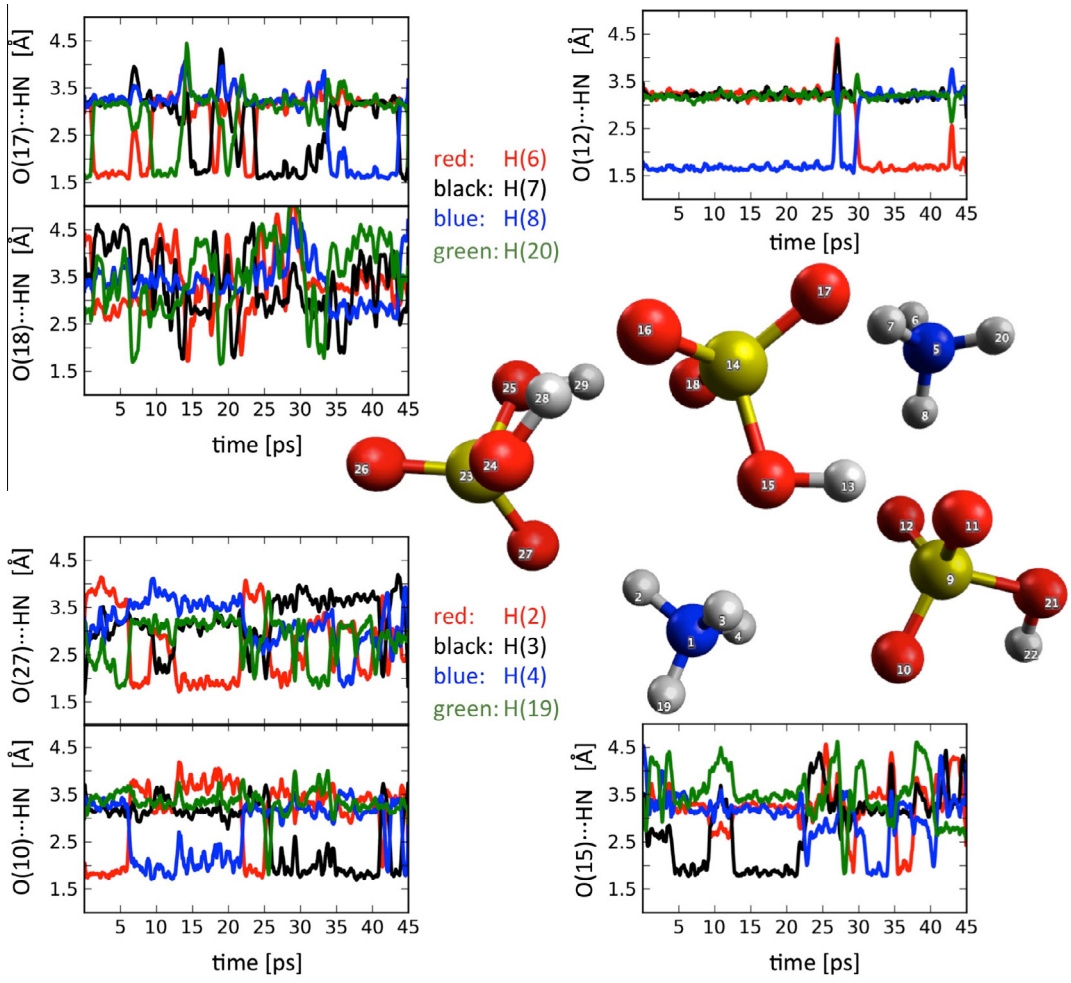

Fig. 6. H-bond fluctuation in the cluster of $(SA)_3(Amm)_2$. The graphs show some of the distances from the hydrogens of the two NH_4^+ molecules to the oxygen atoms of the surrounding bisulfate/sulfuric acid molecules, demonstrating the dynamical nature of the hydrogen bonding in the clusters. Notice that the bonding pattern is conserved regardless of the molecular rotations.

in the clusters of $(SA)_n(base)_{n-1}$ the intact sulfuric acid molecule is always coordinated by more than just one molecule. The high-level of coordination is not unexpected, as we are intentionally studying very stable cluster configurations. It should be noted that most of the studied clusters are not direct collision products of sulfuric acid, ammonia, dimethylamine molecules or even $(SA)_1(base)_1$ units. Rather, the initial clusters were configurations of the constituent molecules which minimize the potential energy at temperature of $T = 0$ K. The results presented in this section show that the clusters seem to be stable at the temperature of $T = 300$ K as well – the thermal energy keeps the molecules vibrating and rotating, but is not enough to break the clusters or significantly transform the geometries away from the very stable static structures.

Molecular dynamics simulations performed in the *NVT* ensemble allow the assessment of the isochoric heat capacity C_V via potential energy fluctuations:

$$C_V = \langle (\Delta E_{pot}^{eq})^2 \rangle / k_B T^2, \quad (1)$$

where $\langle (\Delta E_{pot}^{eq})^2 \rangle$ is the variance of the potential energy during the equilibrium simulations, k_B is the Boltzmann constant and T the temperature. The heat capacities of all the studied clusters are given in Table 2. The uncertainty in the heat capacities is difficult to estimate and it should be kept in mind that the C_V calculated from an *NVT* simulation depends on the thermostat settings. To obtain a crude estimate how the length of the simulation period affects the C_V values, we divided the equilibrium period of 35 ps into blocks of six different sizes: 5 ps, 5.85 ps, 7 ps, 8.75 ps, 11.76 ps and 17.5 ps, thus fitting into the equilibrium period six, five, four, three and two times, respectively. We then evaluated the heat capacities and obtained standard deviations within each block size. Finally, we took the weighted average of the standard deviations as the uncertainty for the final heat capacity, evaluated using the whole equilibrium simulation.

The heat capacities of the ammonia-containing clusters do not show particular systematics with regard to the system size. In contrast, the heat capacity of the amine clusters increases with increasing cluster size. At least partly this is explained by the larger size of the dimethylamine molecule in comparison with the ammonia molecule. Table 2 also contains the heat capacities for all the clusters obtained via structure optimization and the rigid rotor–harmonic oscillator approximation at two different levels of theory: PBE density functional with polarized triple-ζ-Gaussian-type basis set and B3LYP hybrid functional [37] with CBSB7 basis set [38]. The former method is very close to the one used here in the FPMD simulations and the latter has been previously used in several atmospheric cluster studies [18,19,21]. All the static calculations were performed with Gaussian 09 program suite [39] and the cluster structures for the optimizations were taken from the equilibrium simulations.

It is interesting to compare the first-principles molecular dynamics simulations results with the static values. The static heat

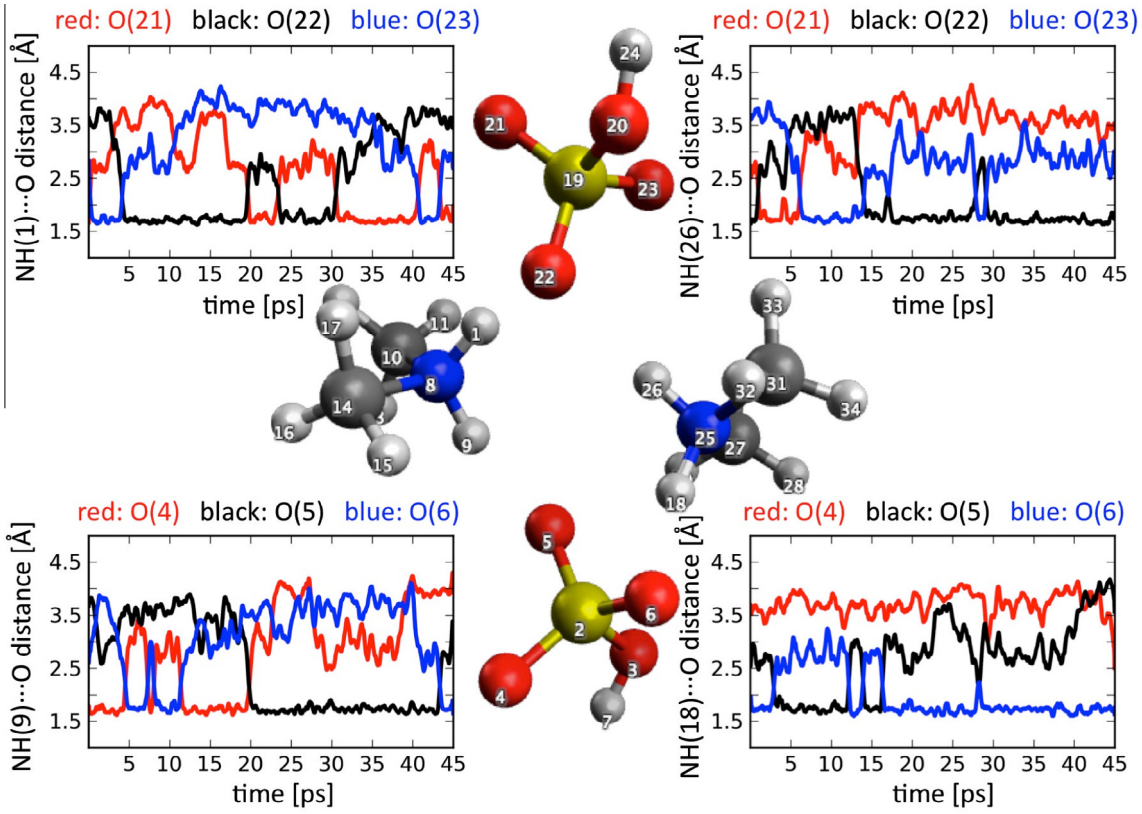

Fig. 7. H-bond fluctuation in the cluster of $(SA)_2(DMA)_2$. The graphs show how the four hydrogen bonds between the sulfuric acid and dimethylamine molecules evolve in time. Notice that the bonding pattern is conserved regardless of the molecular rotations.

Table 2
Heat capacities $\frac{C_V}{\text{molecule}}$ [$\frac{\text{cal}}{\text{mol}}$/K] from the first-principles molecular dynamics simulations at the temperature $T = 300$ K (the column "FPMD"). For comparison, heat capacities from static calculations at two different levels of theory are also shown (see text).

Cluster	FPMD	PBE/TZVP	B3LYP/CBSB7
$(SA)_2(Amm)_1$	17.1 ± 0.9	16.4	15.9
$(SA)_3(Amm)_2$	20.0 ± 2.4	16.0	15.6
$(SA)_3(Amm)_3$	17.3 ± 1.0	15.0	14.7
$(SA)_4(Amm)_3$	20.6 ± 0.7	16.0	15.6
$(SA)_2(DMA)_1$	23.1 ± 1.0	19.4	18.8
$(SA)_2(DMA)_2$	24.3 ± 1.0	19.6	19.1
$(SA)_3(DMA)_3$	27.0 ± 0.9	19.4	18.9
$(SA)_4(DMA)_4$	29.7 ± 2.5	19.7	19.2

capacities are quite uniform within the both sets of clusters – both methods yielding 3–4 kcal/mol larger C_V for the amine clusters and neither capturing the increasing trend for the amine-containing clusters. The main contribution to the static heat capacities comes from the vibrational frequencies, here assumed to be harmonic. Clearly, to capture the thermal movement of the clusters in equilibrium one needs to go beyond the harmonic approximation. This is in concert with the earlier observation that there is anharmonicity in the energetics of the clusters (cf. Table 1) and further, the anharmonicity grows with the system size.

3.2. Dipole moments and vibrational spectra

The interactions between the clusters presented are notoriously weak. In particular in the case of electrically neutral clusters there are no chemical reactions besides proton transfer and the strongest bond between the species is the hydrogen bond. In this landscape the van der Waals interactions become important. For example, it is probable that the electric dipole moment has a role in the collisions between neutral clusters. However, not much is known about the dipoles of the clusters under study. To address this, we have calculated the time-evolution of the electric dipole moments for all the clusters under study.

The first-principles molecular dynamics simulations yielded phase-space trajectories for all the atomic nuclei. We took "snapshots" of these trajectories with an interval of 5 fs and found an approximative location for the negative charge using maximally localized Wannier function centers [40,41]. Knowing the locations of the positive and negative charges, we were able to calculate the electric dipole moments. The dipole moments of all the studied clusters are shown in Fig. 8; the ammonia-containing clusters are on the left pane and the dimethylamine-containing clusters on the right.

Again, there are at least two interesting features in Fig. 8. There is fast, large-amplitude oscillation around the momentary mean values. But unlike in the case of potential energy, here also the mean values are oscillating, although with slower frequency and smaller magnitude. The reason for this undulatory behavior is the same as for the potential energy and bond distance oscillation: thermal molecular movement. However, it seems that the dipole moment is more sensitive than the potential energy to molecular movement. For example, the thermal rotations taking place within the equilibrium bonding patterns do not show up in the potential energy (cf. Figs. 1, 2, 6 and 7), but these rotations are likely to contribute to the fluctuations seen in the electric dipoles (cf. Fig. 8).

The equilibrium values of the electric dipole moments are summarized in Table 3. The cluster data set is too limited in order to draw general systematic conclusions about the dipole moments. However, it is interesting to notice that the electric dipole

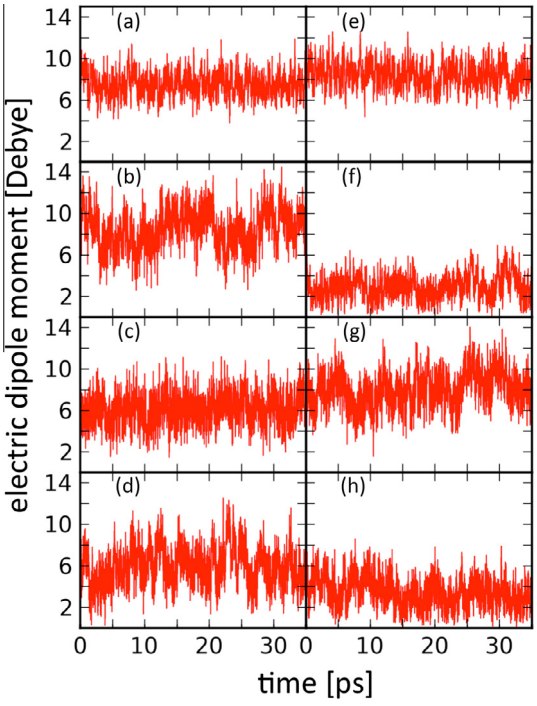

Fig. 8. Electric dipole moments of the studied clusters as a function of time. The time axis corresponds to the last 35 ps of the simulations. (a) $(SA)_2(Amm)_1$, (b) $(SA)_3(Amm)_2$, (c) $(SA)_3(Amm)_3$, (d) $(SA)_4(Amm)_3$, (e) $(SA)_2(DMA)_1$, (f) $(SA)_2(DMA)_2$, (g) $(SA)_3(DMA)_3$ and (h) $(SA)_4(DMA)_4$.

moments of dimethylamine-containing clusters with an even number of acids and bases are considerably smaller than those with an odd number of bases, probably due to symmetry in clusters. The ammonia-clusters do not show similar characteristics.

The electric dipole moment is related to the vibrational–rotational spectrum of the clusters. The thermal fluctuation seen in the dipoles is bound to also have an effect on the spectra of the clusters. To obtain the IR absorption power spectrum $I(\omega)$, we Fourier transformed the autocorrelation function of the electric dipole moment $M(t)$ [42]:

$$I(\omega) \propto \omega \tanh(\beta\hbar\omega/2) \int dt\ e^{-i\omega t} \langle M(t)M(0)\rangle_{eq}, \qquad (2)$$

where $1/\beta = k_B T$ and $k_B, \hbar$ are the Boltzmann and Planck constants, respectively, and T is the temperature. The angular brackets denote the autocorrelation function of the electric dipole moment $M(t)$ taken over the equilibrium simulation with a maximum time-shift of 17.5 ps.

The spectra $I(\omega)$ for all the clusters is shown in Fig. 9. One should note that 35 ps of equilibrium simulation is rather short period for full spectrum analysis; thus the lower-end of the spectra shown here tends to be noisy. Also, the 5 fs interval for evaluating the dipoles limits the high-frequency end of the spectrum, and furthermore, the thermostat coupling constant of 2000 cm^{-1} makes the higher-end of the spectra less reliable. Indeed, the spectra are not shown here out of spectroscopic interest, but rather because they provide yet another view on the thermal molecular motion. The harmonic vibrational spectra are also shown for comparison. Fig. 9 reveals immediately that IR spectroscopy in general is not the most useful tool to study the clusters of sulfuric acid with ammonia or dimethylamine; all the vibrations are centered at two regions, one from the very low end up to 1750 cm^{-1} and another centered below 3000 cm^{-1}. This renders the spectra practically indistinguishable from one another. However, pertinent to the current paper are the differences in the FPMD and harmonic spectra. These differences are a manifestation of the difference in the two approaches, using static structures or performing molecular dynamics simulations. Importantly, in the former approach the inclusion of all the thermal quantities is typically done via the harmonic vibrational frequencies – how well these represent true vibrations is directly related to the reliability of the entropic contribution to the free energies. As can be seen from Fig. 9, the two types of spectra are not identical, but on the other hand, the spectra are not completely different either. The spectra from FPMD simulations are more disperse and consist of numerous peaks, whereas the harmonic spectra consist of sharp and well-defined peaks. As stated in Section 3.1, in the simulations at $T = 300$ K the molecules are under constant thermal motion. All of this motion constitutes

Table 3
Mean values of the electric dipole moments from the first-principles molecular dynamics simulations, corresponding to the last 35 ps of simulations in Figs. 1 and 2. The electric dipole moments are calculated with an interval of 5 fs.

Cluster	Electric dipole moment [Debye]
$(SA)_2(Amm)_1$	7.6 ± 1.1
$(SA)_3(Amm)_2$	8.5 ± 1.9
$(SA)_3(Amm)_3$	6.1 ± 1.5
$(SA)_4(Amm)_3$	5.9 ± 1.8
$(SA)_2(DMA)_1$	8.5 ± 1.2
$(SA)_2(DMA)_2$	2.9 ± 1.2
$(SA)_3(DMA)_3$	8.1 ± 1.7
$(SA)_4(DMA)_4$	3.6 ± 1.4

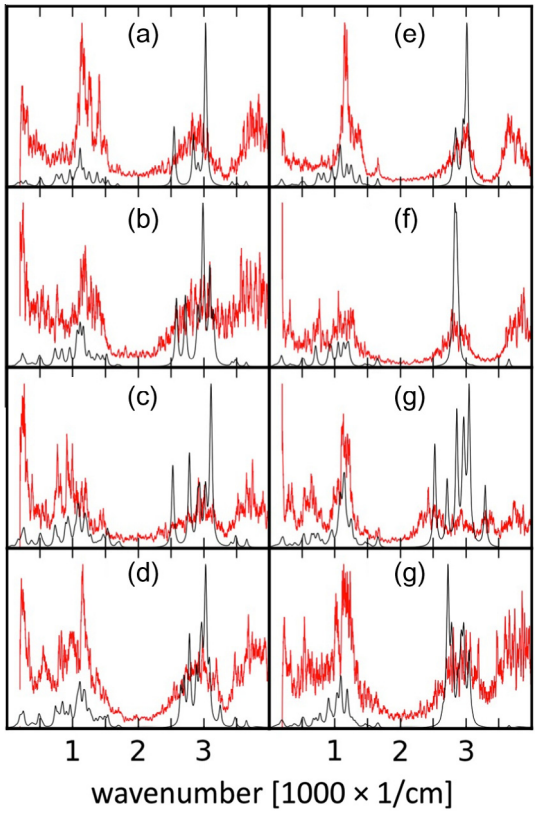

Fig. 9. The IR absorption spectra for all the studied clusters. The spectra in red are obtained from the first-principles molecular dynamics simulations as described in the text. The spectra shown in black are calculated from single static structures within the harmonic approximation using Gaussian 09 program suite [39] at the PBE/TZVP level of theory. (a) $(SA)_2(Amm)_1$, (b) $(SA)_3(Amm)_2$, (c) $(SA)_3(Amm)_3$, (d) $(SA)_4(Amm)_3$, (e) $(SA)_2(DMA)_1$, (f) $(SA)_2(DMA)_2$, (g) $(SA)_3(DMA)_3$ and (h) $(SA)_4(DMA)_4$. (For interpretation of the references to color in this figure legend, the reader is referred to the web version of this article.)

the vibrational spectrum of the cluster in question – including the thermal rotations within the clusters, which are beyond the harmonic approach. However, in this particular study, the proton transfer patterns strongly lock the cluster geometries, and the molecular motion takes place around these dynamical equilibrium geometries. Fig. 9 shows that this motion is not harmonic. In other words, in FPMD simulations the atomic nuclei are not "sitting in harmonic wells" but move more dynamically.

4. Conclusions

We have performed first-principles molecular dynamics simulations to obtain insight into the dynamics and stability of small (sulfuric acid)(ammonia/dimethylamine) clusters. The studied clusters represent prototype examples of stabilized atmospheric sulfuric acid clusters, and as such their properties are important for the formation and further growth of atmospheric aerosol particles. Based on the FPMD simulations, the following conclusions can be drawn:

(a) the kinetic energy at $T = 300$ K keeps the molecules constantly moving – as a consequence, a whole distribution of cluster geometries become relevant, rather than just one minimum energy cluster configuration;
(b) regardless of this movement, the clusters stay bound together – there are no signs of protons transferring back to sulfuric acid molecules from the base molecules or the intact sulfuric acid molecules leaving the clusters;
(c) the electric dipole moments are sensitive to the molecular movement and show large fluctuations; and
(d) the vibrational–rotational spectra of the clusters clearly differ from the harmonic one – demonstrating that the thermal molecular movement in FPMD simulations is not harmonic.

It is worth emphasizing that the initial cluster configurations were products of configuration space sampling and optimization routines, not simple agglomerates of direct molecular collisions. This is an important detail, as the simulations here show that the studied clusters are also rather stable when the effect of kinetic energy is explicitly considered. Now, the interesting question is: do these stable clusters exist in the atmosphere? Or perhaps more accurately, do these stable clusters dominate the cluster configuration distribution for a given cluster composition? To answer these questions is beyond the scope of the present paper. However, the results presented here are intimately related to these issues. For example, when a cluster of one sulfuric acid and one dimethylamine molecule forms, one proton transfer most probably takes place. The potential energy of the complex decreases significantly, thus increasing the kinetic energy. It is plausible that the collisions with the carrier gas take away the excess kinetic energy from the cluster, after which it would evolve as the larger clusters simulated in this paper. However, the formation dynamics of the larger clusters are much more uncertain. As shown here, the bonding patterns of the clusters are rather stable, but for example to go from the cluster of $(SA)_2(DMA)_2$ to $(SA)_3(DMA)_3$ cluster, or from $(SA)_3(DMA)_3$ to $(SA)_4(DMA)_4$, requires breaking the bonding patterns and rearranging the molecules. Typically, it has been assumed that the rearrangement is instantaneous and barrierless. The FPMD simulation results presented here suggest that this might not be the case. From a more applicative point-of-view, these issues would serve to effectively lower the stability of the clusters in terms of formation free energy, as calculated by the standard quantum chemical procedure. Also, the observed distribution of cluster configurations at the temperature of $T = 300$ K and the increasing anharmonicity with growing cluster size are likely to work in the same direction. These interesting questions shall be the focus of the future investigations.

Acknowledgments

This work was financially supported by the Maj and Tor Nessling Foundation (project #2011200), the Academy of Finland (Center of Excellence program project #1118615, LASTU program project #135054) and the European Research Council (project ERC-StG 257360-MOCAPAF). We also thank the Livermore Computing and the Grand Challenge scientific computing program and the CSC – IT Center for Science Ltd for kindly providing computer resources. Part of this work was performed under the auspices of the US Department of Energy under contract DE-AC52–07NA27344.

Appendix A. Supplementary data

Supplementary data associated with this article can be found, in the online version, at http://dx.doi.org/10.1016/j.chemphys.2013.11.014.

References

[1] D.T. Shindell, H. Levy II, M.D. Schwarzkopf, L.W. Horowitz, J.-F. Lamarque, G. Faluvegi, J. Geophys. Res. 113 (2008) D11109.
[2] M.B. Baker, T. Peter, Nature 451 (2008) 299.
[3] M. Kulmala, A. Asmi, H.K. Lappalainen, U. Baltensperger, J.-L. Brenguier, M.C. Facchini, H.-C. Hansson, Ø. Hov, C.D. O'Dowd, U. Pöschl, A. Wiedensohler, R. Boers, O. Boucher, G. de Leeuw, H.A.C. Denier van der Gon, J. Feichter, R. Krejci, P. Laj, H. Lihavainen, U. Lohmann, G. McFiggans, T. Mentel, C. Pilinis, I. Riipinen, M. Schulz, A. Stohl, E. Swietlicki, E. Vignati, C. Alves, M. Amann, M. Ammann, S. Arabas, P. Artaxo, H. Baars, D.C.S. Beddows, R. Bergström, J.P. Beukes, M. Bilde, J.F. Burkhart, F. Canonaco, S.L. Clegg, H. Coe, S. Crumeyrolle, B. D'Anna, S. Decesari, S. Gilardoni, M. Fischer, A.M. Fjaeraa, C. Fountoukis, C. George, L. Gomes, P. Halloran, T. Hamburger, R.M. Harrison, H. Herrmann, T. Hoffmann, C. Hoose, M. Hu, A. Hyvärinen, U. Hõrrak, Y. Iinuma, T. Iversen, M. Josipovic, M. Kanakidou, A. Kiendler-Scharr, A. Kirkevåg, G. Kiss, Z. Klimont, P. Kolmonen, M. Komppula, J.-E. Kristjánsson, L. Laakso, A. Laaksonen, L. Labonnote, V.A. Lanz, K.E.J. Lehtinen, L.V. Rizzo, R. Makkonen, H.E. Manninen, G. McMeeking, J. Merikanto, A. Minikin, S. Mirme, W.T. Morgan, E. Nemitz, D. O'Donnell, T.S. Panwar, H. Pawlowska, A. Petzold, J.J. Pienaar, C. Pio, C. Plass-Duelmer, A.S.H. Prévôt, S. Pryor, C.L. Reddington, G. Roberts, D. Rosenfeld, J. Schwarz, Ø. Seland, K. Sellegri, X.J. Shen, M. Shiraiwa, H. Siebert, B. Sierau, D. Simpson, J.Y. Sun, D. Topping, P. Tunved, P. Vaattovaara, V. Vakkari, J.P. Veefkind, A. Visschedijk, H. Vuollekoski, R. Vuolo, B. Wehner, J. Wildt, S. Woodward, D.R. Worsnop, G.-J. van Zadelhoff, A.A. Zardini, K. Zhang, P.G. van Zyl, V.-M. Kerminen, K. S Carslaw, S.N. Pandis, Atmos. Chem. Phys. 11 (2011) 13061.
[4] M. Kulmala, H. Vehkamäki, T. Petäjä, M. Dal Maso, A. Lauri, V.-M. Kerminen, W. Birmili, P.H. McMurry, Aerosol Sci. 35 (2004) 143.
[5] M. Sipilä, T. Berndt, T. Petäjä, D. Brus, J. Vanhanen, F. Stratmann, J. Patokoski, R.L. Mauldin III, A.-P. Hyvärinen, H. Lihavainen, M. Kulmala, Science 327 (2010) 1243.
[6] R. Zhang, Science 328 (2010) 1366.
[7] C. Kuang, I. Riipinen, S.-L. Sihto, M. Kulmala, A.V. McCormick, P.H. McMurry, Atmos. Chem. Phys. 10 (2010) 8469.
[8] M. Kulmala, L. Pirjola, J.M. Mäkelä, Nature 404 (2000) 66.
[9] F. Yu, R.P. Turco, J. Geophys. Res. 106 (2001) 4797.
[10] H.E. Manninen, T. Nieminen, E. Asmi, S. Gagné, S. Häkkinen, K. Lehtipalo, P. Aalto, M. Vana, A. Mirme, S. Mirme, U. Hõrrak, C. Plass-Dülmer, G. Stange, G. Kiss, A. Hoffer, N. Törő, M. Moerman, B. Henzing, G. de Leeuw, M. Brinkenberg, G.N. Kouvarakis, A. Bougiatioti, N. Mihalopoulos, C. O'Dowd, D. Ceburnis, A. Arneth, B. Svenningsson, E. Swietlicki, L. Tarozzi, S. Decesari, M.C. Facchini, W. Birmili, A. Sonntag, A. Wiedensohler, J. Boulon, K. Sellegri, P. Laj, M. Gysel, N. Bukowiecki, E. Weingartner, G. Wehrle, A. Laaksonen, A. Hamed, J. Joutsensaari, T. Petäjä, V.-M. Kerminen, M. Kulmala, Atmos. Chem. Phys. 10 (2010) 7907.
[11] J. Kirkby, J. Curtius, J. Almeida, E. Dunne, J. Duplissy, S. Ehrhart, A. Franchin, S. Gagné, L. Ickes, A. Kürten, A. Kupc, A. Metzger, F. Riccobono, L. Rondo, S. Schobesberger, G. Tsagkogeorgas, D. Wimmer, A. Amorim, F. Bianchi, M. Breitenlechner, A. David, J. Dommen, A. Downard, M. Ehn, R.C. Flagan, S. Haider, A. Hansel, D. Hauser, W. Jud, H. Junninen, F. Kreissl, A. Kvashin, A. Laaksonen, K. Lehtipalo, J. Lima, E.R. Lovejoy, V. Makhmutov, S. Mathot, J. Mikkilä, P. Minginette, S. Mogo, T. Nieminen, A. Onnela, P. Pereira, T. Petäjä, R. Schnitzhofer, J.H. Seinfeld, M. Sipilä, Y. Stozhkov, F. Stratmann, A. Tomé, J. Vanhanen, Y. Viisanen, A. Vrtala, P.E. Wagner, H. Walther, E. Weingartner, H. Wex, P.M. Winkler, K.S. Carslaw, D.R. Worsnop, U. Baltensperger, M. Kulmala, Nature 476 (2011) 429.

[12] J.M. Mäkelä, S. Yli-Koivisto, V. Hiltunen, W. Seidl, E. Swietlicki, K. Teinilä, M. Sillanpää, I.K. Koponen, J. Paatero, K. Rosman, K. Hämeri, Tellus 53B (2001) 380.
[13] T. Kurtén, V. Loukonen, H. Vehkamäki, M. Kulmala, Atmos. Chem. Phys. 8 (2008) 4095.
[14] V. Loukonen, T. Kurtén, I.K. Ortega, H. Vehkamäki, A.A.H. Pádua, K. Sellegri, M. Kulmala, Atmos. Chem. Phys. 10 (2010) 4961.
[15] J.N. Smith, K.C. Barsanti, H.R. Friedli, M. Ehn, M. Kulmala, D.R. Collins, J.H. Scheckman, B.J. Williams, P.H. McMurry, Proc. Natl. Acad. Sci. 107 (2010) 6634.
[16] B.R. Bzdek, D.P. Ridge, M.V. Johnston, Atmos. Chem. Phys. 10 (2010) 3495.
[17] J. Zhao, J.N. Smith, F.L. Eisele, M. Chen, C. Kuang, P.H. McMurry, Atmos. Chem. Phys. 11 (2011) 10823.
[18] I.K. Ortega, O. Kupiainen, T. Kurtén, T. Olenius, O. Wilkman, M.J. McGrath, V. Loukonen, H. Vehkamäki, Atmos. Chem. Phys. 12 (2012) 225.
[19] O. Kupiainen, I.K. Ortega, T. Kurtén, H. Vehkamäki, Atmos. Chem. Phys. 12 (2012) 3591.
[20] J.H. Zollner, W.A. Glasoe, B. Panta, K.K. Carlson, P.H. McMurry, D.R. Hanson, Atmos. Chem. Phys. 12 (2012) 4399.
[21] P. Paasonen, T. Olenius, O. Kupiainen, T. Kurtén, T. Petäjä, W. Birmili, A. Hamed, M. Hu, L.G. Huey, C. Plass-Duelmer, J.N. Smith, A. Wiedensohler, V. Loukonen, M.J. McGrath, I.K. Ortega, A. Laaksonen, H. Vehkamäki, V.-M. Kerminen, M. Kulmala, Atmos. Chem. Phys. 12 (2012) 9113.
[22] M. Chen, M. Titcombe, J. Jiang, C. Jen, C. Kuang, M.L. Fischer, F.L. Eisele, J.I. Siepmann, D.R. Hanson, J. Zhao, P.H. McMurry, Proc. Natl. Acad. Sci. 109 (2012) 18713.
[23] T. Kurtén, H. Vehkamäki, Adv. Quantum Chem. 55 (2008) 407.
[24] K.E. Anderson, J.I. Siepmann, P.H. McMurry, J. VandeVondele, J. Am. Chem. Soc. 130 (2008) 14144.
[25] J. VandeVondele, M. Krack, F. Mohamed, M. Parrinello, T. Chassaing, J. Hutter, Comput. Phys. Commun. 167 (2005) 103.
[26] G. Lippert, J. Hutter, M. Parrinello, Mol. Phys. 92 (1997) 477.
[27] J.P. Perdew, K. Burke, M. Ernzerhof, Phys. Rev. Lett. 77 (1996) 3865.
[28] M.J. McGrath, J.I. Siepmann, I.-F.W. Kuo, C.J. Mundy, Mol. Phys. 104 (2006) 3619.
[29] I.-F.W. Kuo, C.J. Mundy, M.J. McGrath, J.I. Siepmann, J. Phys. Chem. C 112 (2008) 15412.
[30] J. Elm, M. Bilde, K.V. Mikkelsen, J. Chem. Theory Comput. 8 (2012) 2071.
[31] H.R. Leverentz, J.I. Siepmann, D.G. Truhlar, V. Loukonen, H. Vehkamäki, J. Phys. Chem. A 117 (2013) 3819.
[32] S. Goedecker, M. Teter, J. Hutter, Phys. Rev. B 54 (1996) 1703.
[33] D.J. Tobias, G.L. Martyna, M.L. Klein, J. Phys. Chem. 97 (1993) 12959.
[34] M.J. McGrath, T. Olenius, K. Ortega, V. Loukonen, P. Paasonen, T. Kurtén, M. Kulmala, H. Vehkamäki, Atmos. Chem. Phys. 12 (2012) 2345.
[35] M. Ehn, H. Junninen, S. Schobesberger, H.E. Manninen, A. Franchin, M. Sipilä, T. Petäjä, V.-M. Kerminen, H. Tammet, A. Mirme, S. Mirme, U. Hõrrak, M. Kulmala, D.R. Worsnop, Aerosol Sci. Technol. 45 (2011) 522.
[36] W.M. Haynes (Ed.), CRC Handbook of Chemistry and Physics, ninety fourth ed., (Internet Version 2014), CRC Press/Taylor and Francis, Boca Raton, FL.
[37] A.D. Becke, J. Chem. Phys. 98 (1993) 5648.
[38] J.A. Montgomery, M.J. Frisch, J.W. Ochterski, J. Chem. Phys. 110 (1999) 2822.
[39] Gaussian 09, Revision A.1, M.J. Frisch, G.W. Trucks, H.B. Schlegel, G.E. Scuseria, M.A. Robb, J.R. Cheeseman, G. Scalmani, V. Barone, B. Mennucci, G.A. Petersson, H. Nakatsuji, M. Caricato, X. Li, H.P. Hratchian, A.F. Izmaylov, J. Bloino, G. Zheng, J.L. Sonnenberg, M. Hada, M. Ehara, K. Toyota, R. Fukuda, J. Hasegawa, M. Ishida, T. Nakajima, Y. Honda, O. Kitao, H. Nakai, T. Vreven, J.A. Montgomery, Jr., J.E. Peralta, F. Ogliaro, M. Bearpark, J.J. Heyd, E. Brothers, K.N. Kudin, V.N. Staroverov, R. Kobayashi, J. Normand, K. Raghavachari, A. Rendell, J.C. Burant, S.S. Iyengar, J. Tomasi, M. Cossi, N. Rega, J.M. Millam, M. Klene, J.E. Knox, J.B. Cross, V. Bakken, C. Adamo, J. Jaramillo, R. Gomperts, R.E. Stratmann, O. Yazyev, A.J. Austin, R. Cammi, C. Pomelli, J.W. Ochterski, R.L. Martin, K. Morokuma, V.G. Zakrzewski, G.A. Voth, P. Salvador, J.J. Dannenberg, S. Dapprich, A.D. Daniels, Farkas, J.B. Foresman, J.V. Ortiz, J. Cioslowski, D.J. Fox, Gaussian Inc, Wallingford CT, 2009.
[40] G.H. Wannier, Phys. Rev. 52 (1937) 191.
[41] P.L. Silvestrelli, M. Bernasconi, M. Parrinello, Chem. Phys. Lett. 277 (1997) 478.
[42] B. Guillot, J. Chem. Phys. 95 (1991) 1543.